Article

Structure

# Structural Basis for the High-Affinity Interaction between CASK and Mint1

## Graphical Abstract

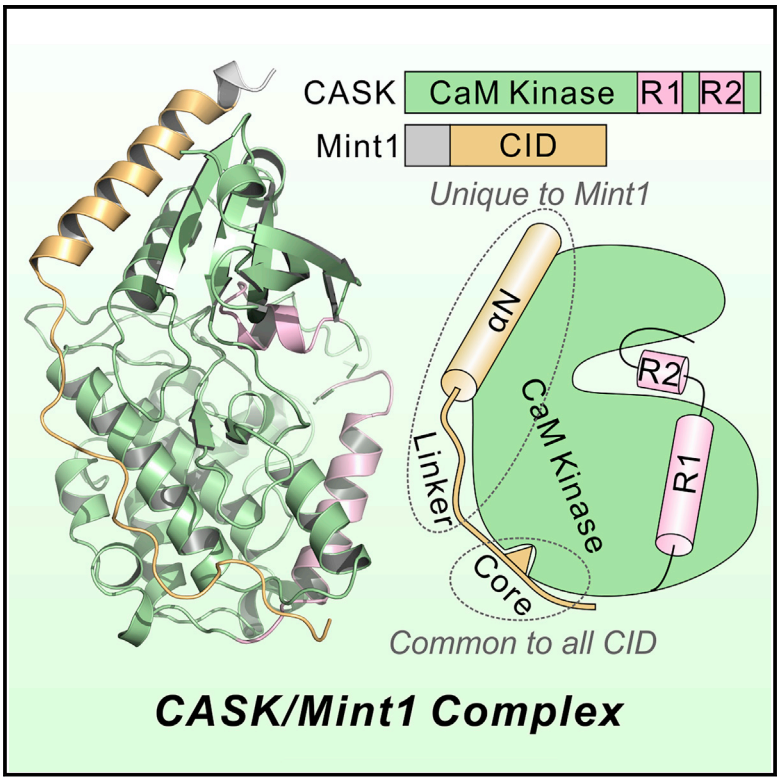


## Highlights

- CASK CaM kinase domain binds to Mint1 with a nanomolar affinity
- An elongated Mint1 fragment wraps around the back side of CaMK
- $Ca^{2+}$/CaM does not affect CASK-CaMK binding to Mint1
- The CASK/Mint1 structure explains some CASK variants found in patients

## Authors

Xiandeng Wu, Qixu Cai, Yiyun Chen, Shihan Zhu, Jing Mi, Jiguang Wang, Mingjie Zhang

## Correspondence

mzhang@ust.hk

## In Brief

Wu et al. discover that an elongated fragment of Mint1/X11α binds to both the N- and C-lobes of CASK-CaMK domain and reveal the mechanism underlying a new mode of highly specific and stable scaffolding role of CASK-CaMK.

Wu et al., 2020, Structure *28*, 664–673
June 2, 2020 
https://doi.org/10.1016/j.str.2020.04.001

CellPress

CellPress

Structure

Article

# Structural Basis for the High-Affinity Interaction between CASK and Mint1

Xiandeng Wu,[1,4] Qixu Cai,[1,4] Yiyun Chen,[1] Shihan Zhu,[1] Jing Mi,[1] Jiguang Wang,[1,2,3] and Mingjie Zhang[1,3,5,*]

[1]Division of Life Science, State Key Laboratory of Molecular Neuroscience, Hong Kong University of Science and Technology, Clear Water Bay, Kowloon, Hong Kong, China

[2]Department of Chemical and Biological Engineering, Hong Kong University of Science and Technology, Clear Water Bay, Kowloon, Hong Kong, China

[3]Center of Systems Biology and Human Health, Hong Kong University of Science and Technology, Clear Water Bay, Kowloon, Hong Kong, China

[4]These authors contributed equally

[5]Lead Contact

*Correspondence: mzhang@ust.hk

https://doi.org/10.1016/j.str.2020.04.001

## SUMMARY

CASK forms an evolutionarily conserved tripartite complex with Mint1 and Veli critical for neuronal synaptic transmission and cell polarity. The CASK CaM kinase (CaMK) domain, in addition to interacting with Mint1, can also bind to many different target proteins, although the mechanism governing CASK-CaMK/target interaction selectivity is unclear. Here, we demonstrate that an extended sequence in the N-terminal unstructured region of Mint1 binds to CASK-CaMK with a dissociation constant of ~7.5 nM. The high-resolution crystal structure of CASK-CaMK in complex with this Mint1 fragment reveals that the C-lobe of CASK-CaMK binds to a short sequence common to known CaMK targets and the N-lobe of CaMK engages an α helix that is unique to Mint1. Biochemical experiments together with structural analysis reveal that the CASK and Mint1 interaction is not regulated by $Ca^{2+}$/CaM. The CASK/Mint1 complex structure provides mechanistic explanations for several CASK mutations identified in patients with brain disorders and cancers.

## INTRODUCTION

Calcium/calmodulin (CaM)-dependent serine protein kinase (CASK), the mammalian ortholog of Lin-2 from *C. elegans*, is a member of the membrane-associated guanylate kinase (MAGUK) family scaffold proteins that are capable of organizing versatile molecular machineries for tissue development and cellular signaling (Hsueh, 2006; Won et al., 2017; Zhu et al., 2016). CASK was initially identified as a neurexin intracellular binding partner in rat brain (Hata et al., 1996), as a *Lin-2* gene product for vulval development in *C. elegans* (Horvitz and Sulston, 1980; Hoskins et al., 1996), and as a gene encoding a protein with an N-terminal CaM kinase-like domain in *Drosophila* brain (Martin and Ollo, 1996). Subsequently, CASK was shown to form a very stable tripartite complex with another two scaffold proteins known as Veli and Mint1 (also known as X11α or Apba1) in the central nervous system as well as in epithelia in mammals (Borg et al., 1998; Butz et al., 1998). This tripartite complex was shown to be highly conserved. The *C. elegans* counterpart of the tripartite complex is formed by Lin-2, Lin-7, and Lin-10, and the complex is critical for polarized targeting of receptor tyrosine kinase LET23 in vulval epithelia (Kaech et al., 1998). The formation of the CASK/Veli/Mint1 complex is mediated by their L27 domains (between CASK and Veli [Feng et al., 2005; Lee et al., 2002]) and by a CASK-CaMK- and Mint1-specific N-terminal unstructured sequence (Borg et al., 1999; Butz et al., 1998) (Figure 1A). A prominent feature of the CASK/Veli/Mint1 complex is that the four PDZ domains, the SH3-GK tandem, and the PTB domain in the complex are not involved in the complex formation and thus are available for binding to various target proteins. Therefore, the CASK/Veli/Mint1 complex can serve as a major organization hub for modulating cellular functions, such as neuronal synaptic transmission, and cell polarity establishment and maintenance. Removal of *CASK* in mice causes animals to die within the first few hours after birth due to tissue development defects, such as impaired palate closure and defects in nervous systems (Atasoy et al., 2007), and with severe kidney development defects in *DLG1* homo- or heterozygous knockout genetic background (Ahn et al., 2013). Perhaps not surprising, mutations of *CASK* have been linked to diseases, including X-linked mental retardation, optic atrophy, kidney function defects, and cancers, in humans (Hsueh, 2009; Moog et al., 2011; Najm et al., 2008).

As a member of the MAGUK family proteins, CASK contains a signature PDZ-SH3-GK tandem (Figure 1A) (Zhu et al., 2016). Distinct from all other MAGUKs, CASK contains a $Ca^{2+}$/CaM-dependent protein kinase (CaMK) domain in its N-terminal end (Figure 1A). The CaMK domain of CASK shares a high sequence identity (~45%) with that of $Ca^{2+}$/CaM-dependent protein kinase II (CaMKII) (Hata et al., 1996). The CASK-CaMK domain was regarded as a pseudo-kinase due to the lack of critical residues for binding to $Mg^{2+}$-ATP in its catalytic site, until it was shown that CASK can function as an $Mg^{2+}$-independent kinase capable of phosphorylating the tail of neurexin, although with a very low kinase activity (Mukherjee et al., 2008, 2010). In addition to functioning as a neurexin kinase, the CaMK domain of CASK is known

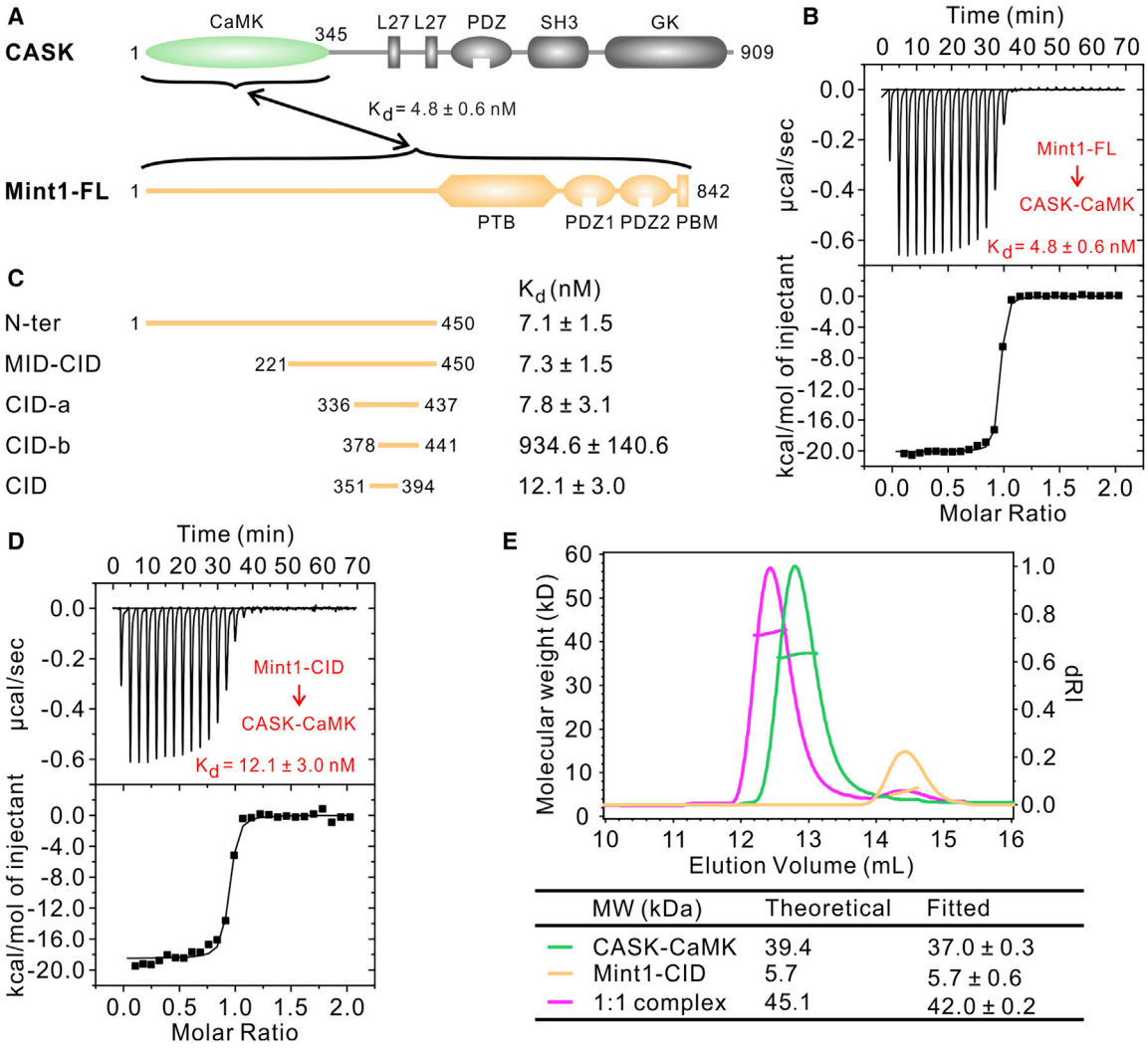


**Figure 1. CASK-CaMK Binds to Mint1-CID with Very High Affinity**

(A) Schematic diagram showing domain organization of CASK and Mint1.

(B) A super-strong interaction between Mint1-FL (amino acids 1–842) and CASK-CaMK (amino acids 1–345) measured by ITC. Mint1-FL (100 μM) in the syringe was titrated into CASK-CaMK (10 μM) in the cell.

(C) Summary of ITC-based measurements of binding affinities between CASK-CaMK and variant fragments of Mint1.

(D) Interaction between CASK-CaMK and Mint1-CID (amino acids 351–394) measured by ITC. Mint1-CID (100 μM) in the syringe was titrated into CASK-CaMK (10 μM) in the cell.

(E) SEC-MALS assay showing the stable and 1:1 stoichiometric complex formation between Mint1-CID and CASK-CaMK. The fitted molecular weights are expressed as the best fitted values ± SE.

to function as an adaptor module capable of binding to many different proteins, including Mint1 (Borg et al., 1998; Butz et al., 1998), Liprins-α (Olsen et al., 2005; Wei et al., 2011), Caskin1 (Stafford et al., 2011; Tabuchi et al., 2002), and TIAM1 (Stafford et al., 2011). Other than the interaction between CASK and Liprins-α (Wei et al., 2011), the structural basis underlying the interactions of CASK-CaMK with these diverse targets remains unclear.

In this study, we discovered that an extended sequence in the N-terminal unstructured region of Mint1 binds to the CASK-CaMK domain with a low nanomolar dissociation constant. The crystal structure of this Mint1 fragment in complex with CASK-CaMK reveals the molecular basis governing the tight and highly specific interaction between CASK and Mint1. Finally, we curated and analyzed numerous CASK variants found in patients with brain disorders or cancers, aiming to provide structural explanations underlying functional defects of some of these *CASK* variants.

## RESULTS

### The N-Terminal Region of Mint1 Binds to CASK-CaMK with a Very High Affinity

It was reported that the CaMK domain of CASK (Figure 1A, termed "CASK-CaMK") was responsible for its interaction with Mint1 (Borg et al., 1999; Butz et al., 1998). We purified CASK-CaMK and the full-length of Mint1 (Figure 1A, termed

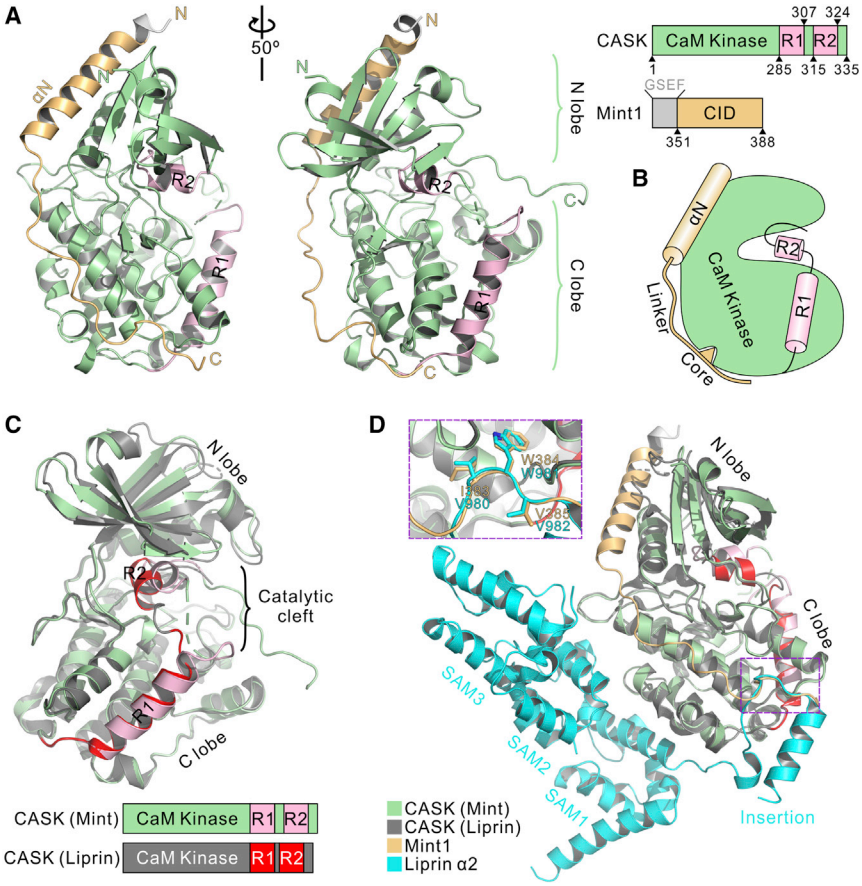


**Figure 2. Crystal Structure of CASK-CaMK in Complex with Mint1-CID**

(A) Ribbon and cartoon representations of the overall structure of CASK-CaMK in complex with Mint1-CID. The coloring scheme is shown in the cartoon diagram in the right panel, and the scheme is used throughout the paper.

(B) Schematic diagram showing the complex structure of CASK-CaMK and Mint1-CID.

(C) Superposition of the CASK-CaMK structures from the CASK/Mint1 complex and the CASK/Liprins-α complex (PDB: 3TAC).

(D) Superposition of the CASK/Mint1 complex and the CASK/Liprins-α complex (PDB: 3TAC) highlighting shared binding mode mediated by the Core region from both Mint1 and Liprins-α (see the enlarged region at the top of the panel).

See also Figure S1.

"Mint1-FL"). Isothermal titration calorimetry (ITC)-based binding assay revealed that CASK-CaMK and Mint1-FL bind to each other with a dissociation constant of about ~4.8 nM (Figure 1B), which is ~100-fold stronger than the binding between CASK-CaMK and Liprins-α (Wei et al., 2011).

We then mapped the minimal CASK binding region of Mint1 by ITC-based quantitative affinity measurements (Figure 1C). The entire N-terminal unstructured region of Mint1 (termed "N-ter") was sufficient for the strong binding to CASK-CaMK. Truncation of the N-terminal half of N-ter (termed "MID-CID" because the region contains both the Munc18 interaction domain and the CASK interaction domain) did not weaken the interaction. We then inspected CASK binding regions reported previously by different groups. An ~100-residue region (CID-a), mapped by Butz et al. (1998), was verified to have the same strong affinity as the entire N-ter did to CASK-CaMK. The CID-b, which was previously mapped as the minimal binding site for CASK (Borg et al., 1999), displayed an ~200-fold decrease in binding to CASK-CaMK compared with Mint1-FL (Figures 1B and 1C). Extending CID-b at the N-terminal end by 27 residues resulted in a Mint1 fragment with a similar CASK-CaMK binding affinity as Mint1 N-ter (Figures 1B–1D). We refer to this minimal CASK binding fragment of Mint1 as Mint1-CID from here on. Size-exclusion chromatography coupled with multi-angle light scattering (SEC-MALS) analysis showed that CASK-CaMK and Mint1-CID formed a stable complex with a 1:1 stoichiometry (Figure 1E).

## Overall Structure of CASK-CaMK in Complex with Mint1-CID

To understand the molecular mechanism governing the super-strong interaction between CASK and Mint1, we solved the crystal structure of CASK-CaMK in complex with Mint1-CID to a resolution of 2.40 Å (Figures 2A and 2B; Table 1). There are three 1:1 stoichiometry complexes in each asymmetric unit of the crystal (Figure S1A). The electron densities are well defined for nearly all residues of both molecules in the complex (V6-P335 for CASK-CaMK and I351-Q388 for Mint1-CID, Figure S1C) except for a short loop (L309-S313) connecting the R1 and R2 helices of CASK-CaMK (Figure 2A). Due to the crystal packing, the four residues ("GSEF") carried over from the cloning vector are also defined (Figures 2A and S1B). The C-terminal tail of CASK-CaMK (i.e., residues following the R2 helix) is also involved in crystal packing with neighboring molecules and shows a well-defined conformation (Figure S1B).

CASK-CaMK in the complex adopts an open conformation that is highly similar to the CASK-CaMK structures from the CASK/3′-AMP complex (Mukherjee et al., 2008) and the CASK/Liprins-α complex (Wei et al., 2011), with root-mean-square deviations of 0.77 and 1.67 Å with the aligned Cα atoms of the kinase domain, respectively (Figure S1D). The CaMK domain in the CASK/Mint1 complex is most open (Figure S1D), probably due to the fact that the insertion of the R2 helix into the nucleotide-binding cleft is deeper in the CASK/Mint1 complex than in the CASK/Liprins-α complex, or 3′-AMP in the CASK/3′-AMP complex (Figures 2C and S1D). Although the CaMK domain in both CASK/Mint1 and CASK/Liprins-α complexes contains an R2 helix (Figure 2C), the residues forming the R2 helices in the two structures are totally different (Figure S1E). Considering that the CaM binding motif overlaps with the R2 sequences of CASK-CaMK in both complexes (Figure S1E) and that $Ca^{2+}$/CaM can bind to the CASK-CaMK/Mint1-CID complex (see below), it is likely that the residues C-terminal to the R1 helix in both CASK/Mint1 and CASK/Liprins-α structures are partially flexible.

**Table 1. Crystallographic Data Collection and Refinement Statistics**

| Data Collection | CASK/Mint1 |
|---|---|
| Space group | $P3_1$ |
| Wavelength (Å) | 0.97853 |
| Unit cell parameters | |
| a, b, c (Å) | 151.417, 151.417, 49.455 |
| α, β, γ (°) | 90, 90, 120 |
| Resolution range (Å) | 50–2.40 (2.44–2.40) |
| No. of unique reflections | 49,568 (2,468) |
| Redundancy | 9.2 (8.6) |
| I/σ | 9.07 (1.39) |
| Completeness (%) | 99.5 (99.3) |
| $R_{merge}$[a] (%) | 16.7 (99.2) |
| $CC_{1/2}$[b] | 0.986 (0.546) |
| **Structure Refinement** | |
| Resolution (Å) | 2.40 |
| $R_{work}$[c] (%) | 17.13 |
| $R_{free}$[d] (%) | 21.29 |
| Root-mean-square deviation | |
| Bonds (Å) | 0.009 |
| Angles (°) | 1.612 |
| Average B factor (Å$^2$) | 30.74 |
| No. of atoms | |
| Protein | 8,730 |
| Ligand/ion | 0 |
| Water | 167 |
| B factors (Å$^2$) | |
| Proteins | 33.1 |
| Ligand/ion | 0 |
| Water | 27.9 |
| Ramachandran plot (%) | |
| Preferred | 95.16 |
| Allowed | 4.74 |
| Outliers | 0.09 |

Numbers in parentheses represent the values for the highest-resolution shell.

[a]$R_{merge} = \Sigma|I_i - \langle I \rangle|/\Sigma I_i$, where $I_i$ is the intensity of measured reflection and $\langle I \rangle$ is the mean intensity of all symmetry-related reflections.

[b]$CC_{1/2}$ was defined in Karplus and Diederichs (2012).

[c]$R_{work} = \Sigma_W||F_{calc}| - |F_{obs}||/\Sigma|F_{obs}|$, where $F_{obs}$ and $F_{calc}$ are observed and calculated structure factors. W is working dataset of about 95% of the total unique reflections randomly chosen and used for refinement.

[d]$R_{free} = \Sigma_T||F_{calc}| - |F_{obs}||/\Sigma|F_{obs}|$, where T is a test dataset of about 5% of the total unique reflections randomly chosen and set aside prior to refinement.

Mint1-CID binds to both the N- and C-lobe of CASK-CaMK, wrapping the back side (relative to the substrate binding site) of the kinase domain (Figure 2B). The structure of Mint1-CID in the complex consists of an N-terminal α helix (termed "αN"), a linker region (defined as "Linker"), and a core region previously identified as the key segment for CASK interaction (termed "Core") (Stafford et al., 2011) (Figures 2A, 2B, S1C, and S2A). Superposition of the CASK/Mint1 structure with the CASK/Liprins-α structure reveals that the insertion sequence between SAM1 and SAM2 of Liprins-α, which is absolutely required for the CASK and Liprins-α interaction (Wei et al., 2011), adopts a similar conformation in binding to the C-lobe of CaMK as Mint1-Core does (Figure 2D), suggesting that Mint1 would prevent Liprins-α from binding to CASK due to Mint1's much stronger affinity toward CASK, which is consistent with previous biochemical data showing the competition between Mint1 and Liprins-α for binding to CASK (LaConte et al., 2016).

## Detailed Interaction between CASK-CaMK and Mint1-CID

The interaction between CASK-CaMK and Mint1-CID can be divided into three interfaces: interface 1 between the N-lobe of CaMK and Mint1-αN, interface 2 between the N- and C-lobe connection region of the CaMK kinase domain and Mint1-Linker, and interface 3 between the C-lobe of CaMK and Mint1-Core (Figures 2B and 3A).

The Mint1-Core binding site on CASK-CaMK is also the core binding region for other kinase domain binding partners, including Liprins-α, Caskin1, and TIAM1 (Stafford et al., 2011; Wei et al., 2011). Three conserved bulky hydrophobic residues in the Mint1-Core (I383, W384, and V385) interact with a pocket in the C-lobe of CASK-CaMK formed by a series of hydrophobic residues, including L99, I103, F111, V112, Y113, V117, Y121, and L149 of CASK (Figures 3B and S2). $W384_{Mint1}$ inserts into the hydrophobic pocket of the kinase domain. Several hydrogen bonds ($R106_{CASK}$/$W384_{Mint1}$, $G110_{CASK}$/$R387_{Mint1}$, $V112_{CASK}$/$V385_{Mint1}$, $N154_{CASK}$/$W384_{Mint1}$, and $Y121_{CASK}$/$W384_{Mint1}$) likely enhance the interaction (Figure 3B). A pair of slat bridge ($E76_{CASK}$/$R371_{Mint1}$) and two hydrogen bonds ($H73_{CASK}$/$Y374_{Mint1}$ and $R123_{CASK}$/$Y374_{Mint1}$) mediate the interaction between CASK-CaMK and Mint1-Linker (Figure 3B).

In interface 1, the N-terminal part of Mint1-CID forms an amphipathic α helix and uses its hydrophobic residues to bind to a hydrophobic surface in the N-lobe of CASK-CaMK (Figures 3C, 3D, and S2C). The interaction between Mint1-αN and CASK-CaMK is unique among the known CASK kinase domain binders. This explains why Mint1 binds to CASK with a much higher affinity than the rest of the binders. Sequence alignment analysis shows that, except for Lin-10 from *C. elegans*, the hydrophobic residues of Mint1-αN are highly conserved from *Drosophila* to higher mammals (Figure S2A).

We used ITC-based experiments to study the contribution of different portions of Mint1-CID to the CASK binding. Mint1-Core binds to CASK-CaMK with a $K_d$ ~0.5 μM (Figure 3E), an affinity comparable with that of the interaction between Liprins-α and CASK (Wei et al., 2011). Addition of Linker to Mint1-Core slightly increased its binding to CASK-CaMK (i.e., removal of αN from Mint1-CID weakened the binding by ~25-fold; Figure 3F). However, the isolated αN-Linker of Mint1 had no detectable binding to CASK-CaMK in the ITC-based assay (Figure 3G). Linking αN-Linker with the Core led to ~40-fold increase in the binding of Mint1 to CASK (Figures 1D versus 3E). ITC-based assay further showed that substitution of $W384_{Mint1}$ by alanine totally abolished the interaction between CASK-CaMK and Mint1-CID (Figure 3H), indicating that Mint1-Core is absolutely required for

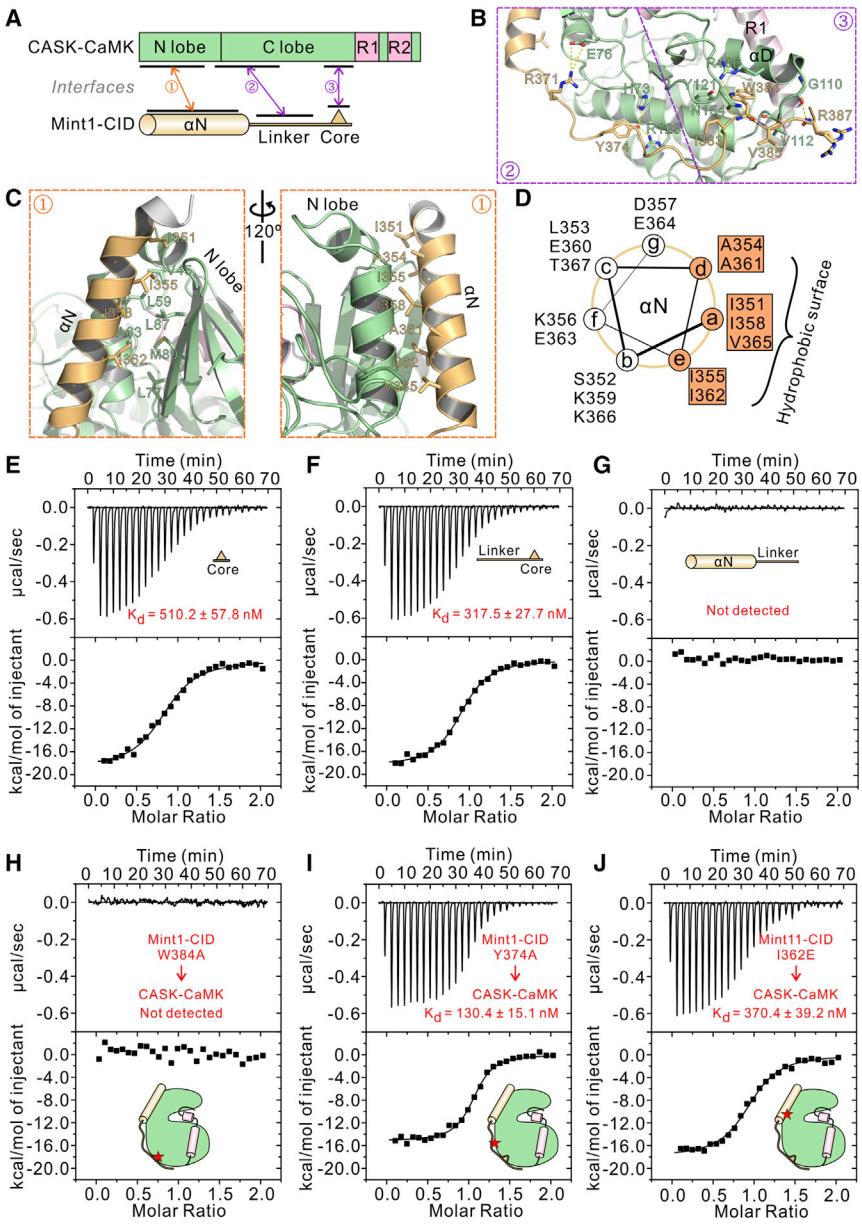


**Figure 3. Detailed Interactions between CASK-CaMK and Mint1-CID**

(A) Schematic diagram showing three binding interfaces between CASK-CaMK and Mint1-CID.

(B) The detailed interactions of interfaces 2 and 3 between CASK-CaMK and Mint1-CID.

(C) The interface 1 between CASK-CaMK and Mint1-CID.

(D) Helical wheel representation showing the hydrophobic surface of Mint1-αN (amino acids 351–367).

(E–G) Interactions between CASK-CaMK and variant fragments of Mint1-CID measured by ITC, including Mint1-Core (amino acids 382–394) (E), Mint1-Linker-Core (amino acids 370–394) (F), and Mint1-αN-Liner (amino acids 351–381) (G). Each Mint1-CID fragment (100 μM) in the syringe was titrated into CASK-CaMK (10 μM) in the cell.

(H–J) Interactions between CASK-CaMK and Mint1-CID mutants measured by ITC: (H) W384A; (I) Y374A; (J) I362E. Each Mint1-CID mutant (100 μM) in the syringe was titrated into CASK-CaMK (10 μM) in the cell.

See also Figures S2.

CASK binding. Replacing $Y374_{Mint1}$ in Mint1-Linker by alanine weakened Mint1-CID binding to CASK by ~10-fold (Figures 3I versus 1D), demonstrating that the Linker region also contributes to the CASK/Mint1 interaction. Substitution of $I362_{Mint1}$ in Mint1-αN by glutamate reduced Mint1-CID binding to CASK by ~20-fold (Figures 3J versus 1D), meaning that this mutation essentially eliminated αN's contribution to the interaction between Mint1-CID and CASK-CaMK (Figures 3J versus 3F).

## The Interaction between CASK and Mint1 Is Not Regulated by $Ca^{2+}$/CaM

Like CaMKII, CASK-CaMK contains a $Ca^{2+}$/CaM binding motif that immediately follows the regulatory R1 helix (Figures 4A and S1E). Structural studies have revealed that the αD helix of CaMKII rotates anti-clockwise by ~30° when the kinase transits from the autoinhibited conformation to the activated conformation (Figure 4A) (Chao et al., 2010; Rellos et al., 2010; Rosenberg et al., 2005). The αD helix of the CASK-CaMK in complex with Mint1-CID adopts the same conformation as αD in the autoinhibited CaMKII (Figure 4A). The structure of the CASK-CaMK in complex with Mint1-CID shows that the R1 helix interacts intimately with αD, shaping the hydrophobic pocket of the kinase C-lobe for binding to Mint1-Core (Figure 3B). Deletion of the R1 helix would remove the restraint of αD imposed by R1 and thus disturb the Mint1-Core binding hydrophobic pocket of the kinase domain. Indeed, truncation of CASK-CaMK by removing both R1 and R2 totally eliminated its binding to Min1-CID (see the next section for more details). The same CASK-CaMK truncation mutant showed no detectable binding to Liprins-α either (Wei et al., 2011).

We then asked whether $Ca^{2+}$/CaM binding to CASK-CaMK might trigger the movement of αD as in the case of CaMKII (Figures 4A and S3A) (Rellos et al., 2010). ITC assay confirmed that the interaction between CaM and CASK is $Ca^{2+}$ dependent (Borg et al., 1999). $Ca^{2+}$/CaM binds to CASK-CaMK with a $K_d$ ~1 μM and apo-CaM has no detectable binding to CASK-CaMK (Figure 4C). However, binding of $Ca^{2+}$/CaM does not impair the complex formation between CASK-CaMK and Mint1-CID as assayed by SEC-MALS analysis (Figures 4D and 4E). It was shown earlier that $Ca^{2+}$/CaM binding does not affect CASK-CaMK binding to Liprins-α (Wei et al., 2011). We also performed an ITC-based quantitative analysis by first saturating CASK-CaMK with $Ca^{2+}$/CaM and then titrating Mint1-CID with the mixture. This analysis showed that binding of $Ca^{2+}$/CaM led

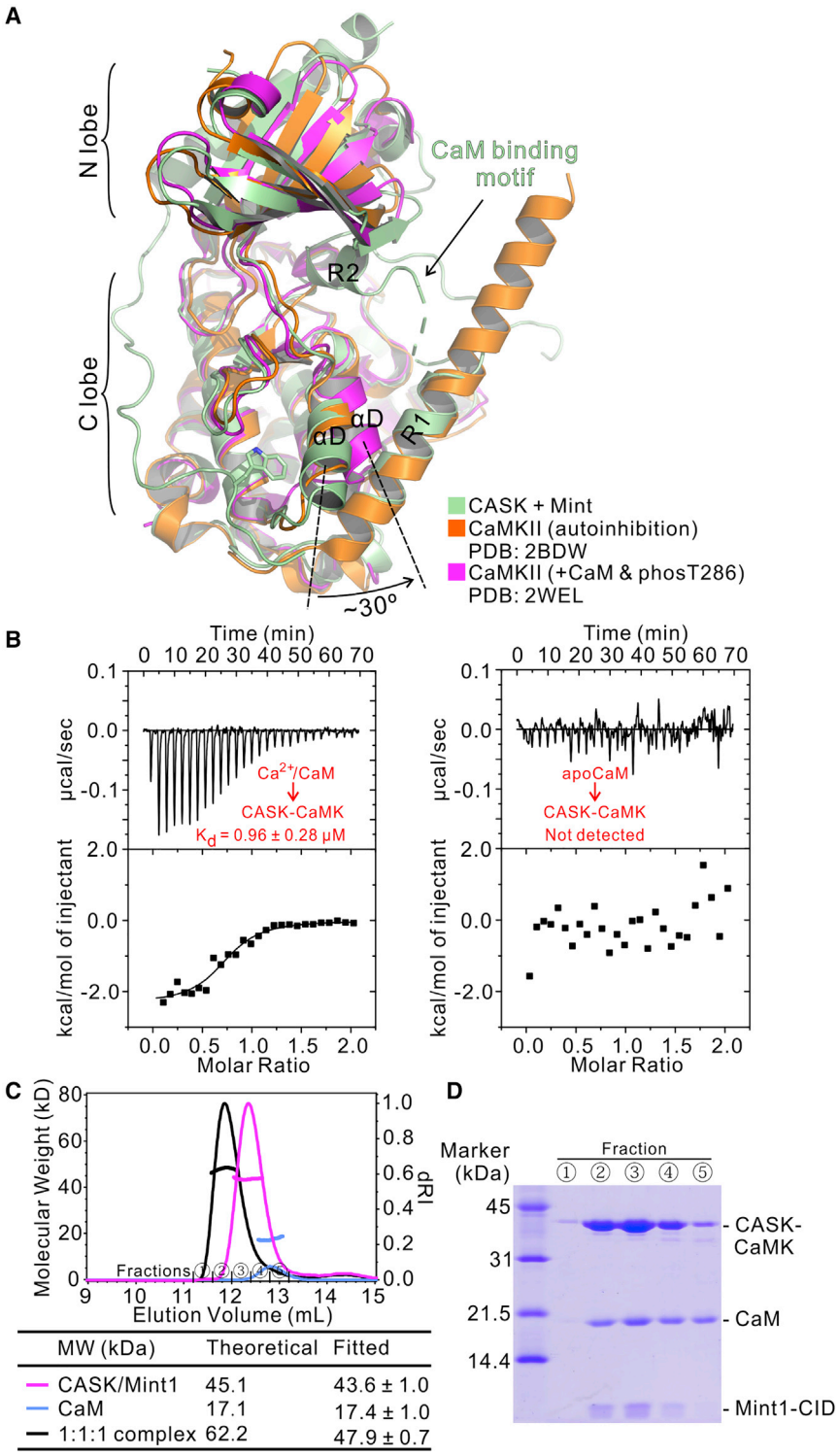


**Figure 4. The Interaction between CASK and Mint1 Is Not Regulated by $Ca^{2+}$/CaM binding to CASK**

(A) Superposition of CASK-CaMK/Mint1 complex with variant CaMKII structures obtained under different conditions, showing the movement of the CaMKII αD helix upon kinase activation.

(B) Interactions between CASK-CaMK and CaM measured by ITC in the presence of $Ca^{2+}$ (left panel) or EDTA condition (right panel) in the assay buffer. CaM (200 μM) in the syringe was titrated into CASK-CaMK (20 μM) in the cell.

(C) SEC-MALS assay showing the complex formation between CASK-CaMK/Mint1-CID and $Ca^{2+}$/CaM. The fitted molecular weights were expressed as the best fitted values ± SE.

(D) SDS-PAGE showing that CASK-CaMK, Mint1-CID, and $Ca^{2+}$/CaM were co-eluted from the size-exclusion column.

See also Figure S3.

to a very mild reduction (~4-fold) of the interaction between CASK-CaMK and Mint1-CID (Figure S3B), indicating that the binding of $Ca^{2+}$/CaM may slightly weaken the interaction between the R1 helix and αD in the CASK kinase domain. Considering CASK-CaMK can bind to a nucleotide (Mukherjee et al., 2008), which may influence the conformation of αD when $Ca^{2+}$/CaM is present, we incorporated AMPPNP in the ITC-based binding experiment. The result showed that AMPPNP did not have obvious impact on the interaction between Mint1-CID and CASK-CaMK saturated by $Ca^{2+}$/CaM (Figure S3C). On the other hand, our experiment demonstrated that deletion of the entire R1 helix (CASK-CaMK 1–277) eliminated Mint1-CID binding (Figure 5D, see below), indicating that the R1 helix is critical for shaping the hydrophobic pocket of the kinase C-lobe for binding to the Mint1-Core, although the R1 helix does not directly contact Mint1-CID. The binding of $Ca^{2+}$/CaM to CASK-CaMK, instead of fully releasing the R1 helix, likely increases the mobility of the R1 helix and consequently slightly weakens its interaction with Mint1-CID. It has been shown that $Ca^{2+}$/CaM binding to CaMKII leads to increase in the conformational flexibility of its R1 helix and consequently promotes the autophosphorylation of T286 of the kinase (Hoffman et al., 2011). Full opening of R1 and consequent anti-clockwise movement of αD in CaMKII may be achieved either by autophosphorylation of T286 in the R1 helix (equivalent to T291 in CASK-CaMK; Figure S1E) (Hoffman et al., 2011; Rellos et al., 2010) or possibly by binding of its substrate to the kinase domain (Figure S3A) (Chao et al., 2010). It remains to be tested whether T291 phosphorylation of, or potential substrate binding to CASK-CaMK may function as a regulatory switch in modulating its binding to target proteins, including Mint1 and Liprins-α.

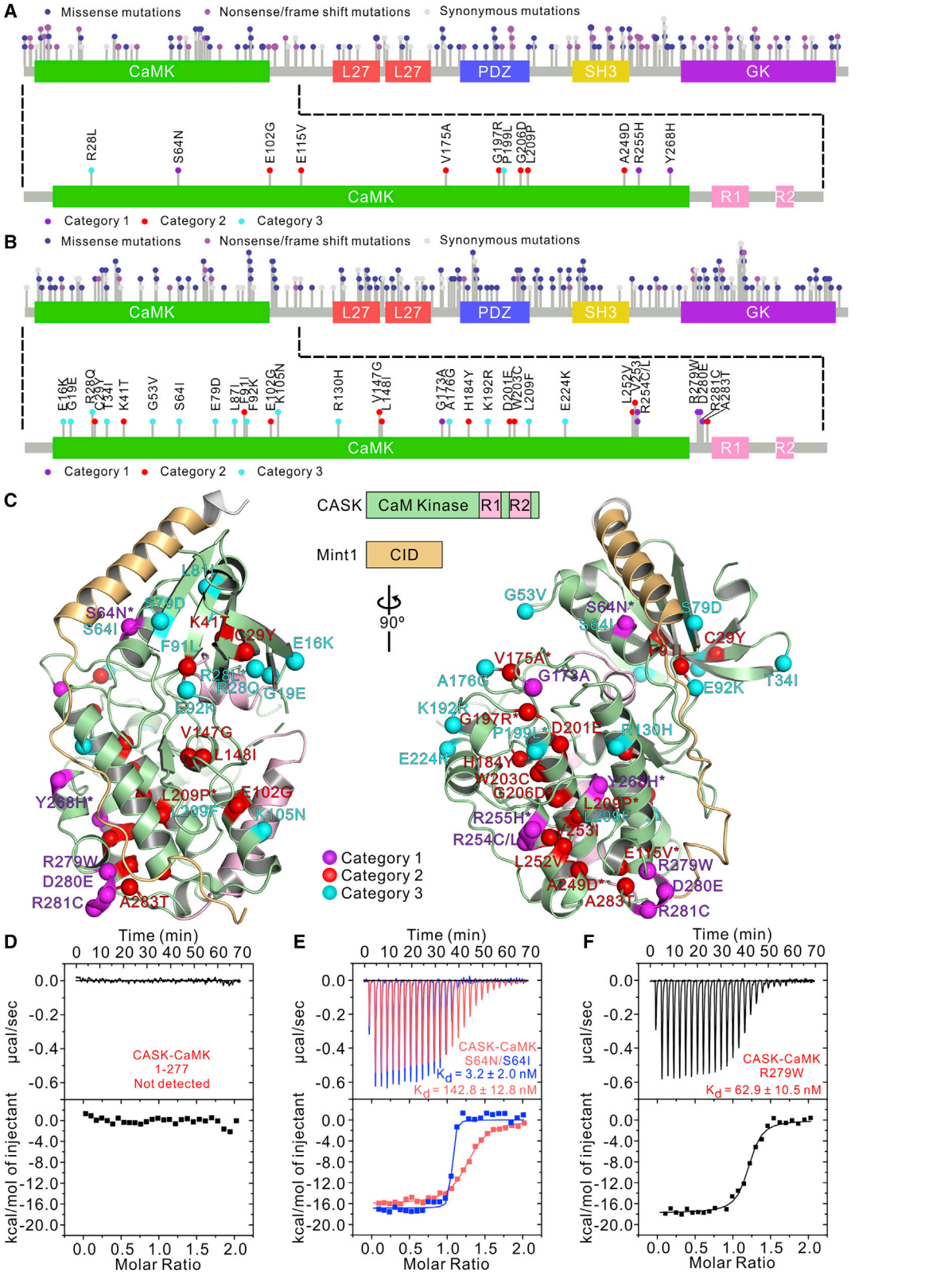


*(legend on next page)*

### Disease Variants Impact CASK-CaMK/Mint1-CID Interaction

We next extracted *CASK* mutations/variants that may be associated with human diseases from several publicly available human genome databases, including ClinVar database (https://www.ncbi.nlm.nih.gov/clinvar/), HGMD database (http://www.hgmd.cf.ac.uk/), and The Cancer Genome Atlas (http://cancergenome.nih.gov/) (Figures 5A and 5B; Tables S1 and S2). A total of 48 missense mutations in 40 residues are located in the CASK-CaMK region. We mapped these missense mutations to the structure of CASK-CaMK/Mint1-CID complex (Figure 5C). We divided the mutations into three categories (Figure 5C). Category 1 includes the mutations of the residues that are directly involved in binding to Mint1-CID or Liprins-α. Category 2 involves residues located in the folding core of the CaMK domain and mutations of these residues are expected to alter the folding of the kinase domain. One of the disease mutation, L209P, associated with microcephaly and bilateral retinal dystrophy plus optic nerve atrophy, was reported to lead to misfolding and insolubility of CASK (LaConte et al., 2019), which is consistent with our structural information. Category 3 concerns the residues on the surface of CaMK but are not directly involved in binding to Mint1 or Liprins-α. We do not have a good explanation for the mutations in category 3 based on the available structures. These mutations may affect other yet unknown binding partners of CASK-CaMK. Alternatively, these mutations may simply be neutral variants of *CASK*.

Using ITC-based binding assays, we measured the impact of several category 1 mutations on CASK's binding to Mint1. The 915G→A *CASK* mutation leads to partial skipping of exon9 (E278–K305, encoding αK, R1, and part of the CaM binding motif of CASK-CaMK), and the mutation is known to be associated with microcephaly (Najm et al., 2008). An earlier study showed that truncation of CASK-CaMK at 277 (CASK-CaMK 1–277) abolished its Liprins-α binding (Wei et al., 2011). Our ITC-based assay showed that the same mutation also abolished CASK-CaMK's binding to Mint1 (Figure 5D). Missense mutations of S64 were identified in patients with brain disorders (S64N) or caner (S64I) (Tables S1 and S2). S64 is in the interface between Mint1-αN and the N-lobe of the CASK kinase domain (Figure 5C). ITC-based assay showed that the S64N mutant of CASK-CaMK showed ~12-fold reduction in binding to Mint1-CID (Figures 5E versus 1D). Curiously, the CASK-CaMK S64I mutant led to ~4-fold stronger binding to Mint1-CID (Figures 5E versus 1D), likely due to enhanced hydrophobic interaction between Mint1-αN and the N-lobe CASK kinase domain (Figure 3C). It is possible that the S64I mutation may be a neutral variant of *CASK*, as the link between *CASK* mutations and cancer is still uncertain. Another CASK mutant (R279W located in the loop connecting the end of the C-lobe and the R1 helix of the kinase domain) found in cancer patients also showed a ~5-fold reduction in binding to Mint1-CID (Figures 5E versus 1D).

## DISCUSSION

In this study, we characterized the biochemical and structural bases underlying the super-strong interaction between CASK and Mint1. We discovered that an elongated fragment from Mint1 interacts with both the N- and C-lobe of the CASK kinase domain, leading to formation of a highly stable CASK/Mint1 complex, which was shown to be resistant to high salt or detergent treatments (Butz et al., 1998). The high-resolution structure of the CASK-CaMK/Mint1-CID revealed that the Mint1-Core uses three continuous hydrophobic residues ("IWV") to bind to a highly conserved hydrophobic surface on the C-lobe of the CASK kinase domain. Importantly, all currently known CASK-CaMK binding proteins contain the similar IWV sequence in each of its CASK kinase domain binding regions (Stafford et al., 2011; Wei et al., 2011). However, Mint1-CID contains a unique N-terminal helix that binds to the N-lobe of the CASK kinase domain, and this N-terminal helix significantly enhances Mint1's binding to CASK, rending Mint1 as the strongest CASK binding partner known to date. Our structural analysis further indicates that the bindings of CASK to Mint1 and to Liprins-α are mutually exclusive (also see LaConte et al., 2016), and Mint1 should have priority in binding to CASK if both Mint1 and Liprins-α exist in a cellular compartment, such as presynaptic buttons. Thus, it is possible that the expression level of Mint1 may be able to regulate the concentration of the CASK/Liprins-α complex and hence synaptic transmission in neuronal synapses.

In addition to functioning as an atypical protein kinase domain capable of phosphorylating neurexin (Mukherjee et al., 2008), our current study further establishes that the CaMK of CASK functions as a versatile adaptor domain binding to many different target proteins. CASK belongs to the CaMKII subfamily of CaMK family proteins. A signature feature for the CaMKII subfamily is that these kinases can respond to cellular calcium concentration changes. $Ca^{2+}$/CaM binds to the autoinhibitory region of CaMKII, leading to activations of the kinases (Bayer and Schulman, 2019; Hell, 2014). $Ca^{2+}$/CaM binding does not seem to regulate CASK-CaMK to bind its target proteins, including Mint1 and Liprins-α, although CASK-CaMK binds $Ca^{2+}$/CaM with a similar affinity as CaMKII (Figure 4). This analysis suggests that the binding of CASK to Mint1 or to Liprins-α is not directly regulated by $Ca^{2+}$ influx into the presynaptic active zones upon arrival of action potentials.

Previous genetic studies have revealed the essential functions of CASK for survival and for neurodevelopment of animals, with

**Figure 5. Disease-Related Variants of CASK found in Patients with Brain Disorders or Cancers**

(A and B) Schematic diagram summarizing the mutations of CASK identified in patients with brain disorders (A) and cancers (B). For simplicity, only the missense mutations in the CASK-CaMK are explicitly labeled. The details of the rest of the mutations can be found in Tables S1 and S2. The sticks with different heights were used to differentiate nearby positions in the sequence.

(C) Mapping of the missense mutations in (A and B) to the structure of the CASK-CaMK/Mint1-CID complex structure. The mutations are divided into three categories as detailed in the text. Mutations from brain disorders were denoted by "*".

(D–F) Bindings of Mint1-CID to various CASK-CaMK mutants. In these measurements, Mint1-CID (100 μM) in the syringe was titrated into each CASK-CaMK mutants (10 μM) in the cell.

See also Tables S1 and S2.

CASK knockout lethal in neonatal mice, and patients with CASK mutations suffering from intellectual disabilities (Atasoy et al., 2007; Hsueh, 2009; Srivastava et al., 2016). In contrast, the functional consequence of the loss of Mint1 is much milder. Neurotransmission defects could only be observed in inhibitory synapses where Mint1 is preferentially expressed, and these defects cannot be explained by possible compensation by other Mint isoforms considering that Mint1 is the only Mint isoform containing CID. The functional compensation between Mint1 and Mint2 in excitatory synapses suggests their additional mode of interaction beyond Mint1's binding to CASK (Ho et al., 2003, 2006). Because CASK binds to many other proteins in addition to Mint1, genetic deletion or mutation of CASK could have obvious deleterious impact on the development of animals. In contrast, Mint1 is only one of many binding partners of CASK that emerged in higher vertebrates during evolution. Accordingly, mutations of Mint1 may display more mild phenotypes in animals.

This study, together with the structure of the CASK-CaMK in complex with the Liprins-$\alpha$ SAM domain in tandem (Wei et al., 2011), provides mechanistic explanations for several CASK mutations that are linked to brain disorders. For example, the S61N and Y268H mutations found in patients with brain disorders are located in the interface between CASK-CaMK and Mint1 or between CASK-CaMK and Liprins-$\alpha$. Mutations of these residues weaken the binding of CASK to either one of the two targets (Figure 5, and Figure 4 in Wei et al., 2011). Our mapping analysis of mutations in the CASK-CaMK region identified in patients with brain disorders or cancers (Figure 5; Tables S1 and S2) may serve as a portal for future studies of CASK in healthy and disease conditions in humans.

## STAR★METHODS

Detailed methods are provided in the online version of this paper and include the following:

- KEY RESOURCES TABLE
- RESOURCE AVAILABILITY
  - Lead Contact
  - Materials Availability
  - Data and Code Availability
- EXPERIMENTAL MODEL AND SUBJECT DETAILS
  - Bacterial Strain
- METHODS DETAILS
  - Constructs, Protein Expression and Purification
  - Protein Crystallization and Structure Determination
- ISOTHERMAL TITRATION CALORIMETRY (ITC) ASSAY
  - Size Exclusion Chromatography Coupled with Multi-Angle Light Scattering (SEC-MALS) Assay
  - Collection of Human Variants Associated with Neurodevelopmental Disorders and Cancer
- QUANTIFICATION AND STATISTICAL ANALYSIS

## SUPPLEMENTAL INFORMATION

Supplemental Information can be found online at https://doi.org/10.1016/j.str.2020.04.001.

## ACKNOWLEDGMENTS

We thank the BL19U1 beamline at National Facility for Protein Science Shanghai (NFPS) for X-ray beam time. This work was supported by grants from RGC of Hong Kong (AoE-M09-12 and C6004-17G) and a grant from the Simons Foundation (award no. 510178) to M.Z. M.Z. is a Kerry Holdings Professor of Science and a Senior Fellow of IAS at HKUST.

## AUTHOR CONTRIBUTIONS

X.W., Q.C., Y.C., S.Z., and J.M. performed the experiments. X.W., Q.C., J.W., and M.Z. analyzed the data. X.W., Q.C., and M.Z. designed the research. X.W., Q.C., and M.Z. drafted the paper and all authors commented on it. M.Z. coordinated the project.

## DECLARATION OF INTERESTS

The authors declare no competing interests.

Received: January 2, 2020
Revised: March 1, 2020
Accepted: April 1, 2020
Published: April 28, 2020

## REFERENCES

Ahn, S.Y., Kim, Y., Kim, S.T., Swat, W., and Miner, J.H. (2013). Scaffolding proteins DLG1 and CASK cooperate to maintain the nephron progenitor population during kidney development. J. Am. Soc. Nephrol. *24*, 1127–1138.

Atasoy, D., Schoch, S., Ho, A., Nadasy, K.A., Liu, X., Zhang, W., Mukherjee, K., Nosyreva, E.D., Fernandez-Chacon, R., Missler, M., et al. (2007). Deletion of CASK in mice is lethal and impairs synaptic function. Proc. Natl. Acad. Sci. U S A *104*, 2525–2530.

Bayer, K.U., and Schulman, H. (2019). CaM kinase: still inspiring at 40. Neuron *103*, 380–394.

Borg, J.-P., Lõpez-Figueroa, M.O., de Taddèo-Borg, M., Kroon, D.E., Turner, R.S., Watson, S.J., and Margolis, B. (1999). Molecular analysis of the X11–mLin-2/CASK complex in brain. J. Neurosci. *19*, 1307–1316.

Borg, J.P., Straight, S.W., Kaech, S.M., de Taddeo-Borg, M., Kroon, D.E., Karnak, D., Turner, R.S., Kim, S.K., and Margolis, B. (1998). Identification of an evolutionarily conserved heterotrimeric protein complex involved in protein targeting. J. Biol. Chem. *273*, 31633–31636.

Butz, S., Okamoto, M., and Südhof, T.C. (1998). A tripartite protein complex with the potential to couple synaptic vesicle exocytosis to cell adhesion in brain. Cell *94*, 773–782.

Chao, L.H., Pellicena, P., Deindl, S., Barclay, L.A., Schulman, H., and Kuriyan, J. (2010). Intersubunit capture of regulatory segments is a component of cooperative CaMKII activation. Nat. Struct. Mol. Biol. *17*, 264–272.

Chen, V.B., Arendall, W.B., 3rd, Headd, J.J., Keedy, D.A., Immormino, R.M., Kapral, G.J., Murray, L.W., Richardson, J.S., and Richardson, D.C. (2010). MolProbity: all-atom structure validation for macromolecular crystallography. Acta Crystallogr. D Biol. Crystallogr. *66*, 12–21.

Ellrott, K., Bailey, M.H., Saksena, G., Covington, K.R., Kandoth, C., Stewart, C., Hess, J., Ma, S., Chiotti, K.E., McLellan, M., et al. (2018). Scalable open science approach for mutation calling of tumor exomes using multiple genomic pipelines. Cell Syst. *6*, 271–281.e7.

Emsley, P., Lohkamp, B., Scott, W.G., and Cowtan, K. (2010). Features and development of Coot. Acta Crystallogr. D Biol. Crystallogr. *66*, 486–501.

Feng, W., Long, J.F., and Zhang, M. (2005). A unified assembly mode revealed by the structures of tetrameric L27 domain complexes formed by mLin-2/mLin-7 and Patj/Pals1 scaffold proteins. Proc. Natl. Acad. Sci. U S A *102*, 6861–6866.

Hata, Y., Butz, S., and Sudhof, T.C. (1996). CASK: a novel dlg/PSD95 homolog with an N-terminal calmodulin-dependent protein kinase domain identified by interaction with neurexins. J. Neurosci. *16*, 2488–2494.

Hell, J.W. (2014). CaMKII: claiming center stage in postsynaptic function and organization. Neuron *81*, 249–265.

Ho, A., Morishita, W., Atasoy, D., Liu, X., Tabuchi, K., Hammer, R.E., Malenka, R.C., and Sudhof, T.C. (2006). Genetic analysis of Mint/X11 proteins: essential presynaptic functions of a neuronal adaptor protein family. J. Neurosci. *26*, 13089–13101.

Ho, A., Morishita, W., Hammer, R.E., Malenka, R.C., and Sudhof, T.C. (2003). A role for Mints in transmitter release: Mint 1 knockout mice exhibit impaired GABAergic synaptic transmission. Proc. Natl. Acad. Sci. U S A *100*, 1409–1414.

Hoffman, L., Stein, R.A., Colbran, R.J., and McHaourab, H.S. (2011). Conformational changes underlying calcium/calmodulin-dependent protein kinase II activation. EMBO J. *30*, 1251–1262.

Horvitz, H.R., and Sulston, J.E. (1980). Isolation and genetic characterization of cell-lineage mutants of the nematode *Caenorhabditis elegans*. Genetics *96*, 435–454.

Hoskins, R., Hajnal, A.F., Harp, S.A., and Kim, S.K. (1996). The *C. elegans* vulval induction gene lin-2 encodes a member of the MAGUK family of cell junction proteins. Development *122*, 97–111.

Hsueh, Y.P. (2006). The role of the MAGUK protein CASK in neural development and synaptic function. Curr. Med. Chem. *13*, 1915–1927.

Hsueh, Y.P. (2009). Calcium/calmodulin-dependent serine protein kinase and mental retardation. Ann. Neurol. *66*, 438–443.

Jay, J.J., and Brouwer, C. (2016). Lollipops in the clinic: information dense mutation plots for precision medicine. PLoS One *11*, e0160519.

Kaech, S.M., Whitfield, C.W., and Kim, S.K. (1998). The LIN-2/LIN-7/LIN-10 complex mediates basolateral membrane localization of the *C. elegans* EGF receptor LET-23 in vulval epithelial cells. Cell *94*, 761–771.

Karplus, P.A., and Diederichs, K. (2012). Linking crystallographic model and data quality. Science *336*, 1030–1033.

LaConte, L.E., Chavan, V., Liang, C., Willis, J., Schonhense, E.M., Schoch, S., and Mukherjee, K. (2016). CASK stabilizes neurexin and links it to liprin-alpha in a neuronal activity-dependent manner. Cell Mol. Life Sci. *73*, 3599–3621.

LaConte, L.E.W., Chavan, V., DeLuca, S., Rubin, K., Malc, J., Berry, S., Gail Summers, C., and Mukherjee, K. (2019). An N-terminal heterozygous missense CASK mutation is associated with microcephaly and bilateral retinal dystrophy plus optic nerve atrophy. Am. J. Med. Genet. A *179*, 94–103.

Landrum, M.J., Lee, J.M., Riley, G.R., Jang, W., Rubinstein, W.S., Church, D.M., and Maglott, D.R. (2013). ClinVar: public archive of relationships among sequence variation and human phenotype. Nucleic Acids Res. *42*, D980–D985.

Lee, S., Fan, S., Makarova, O., Straight, S., and Margolis, B. (2002). A novel and conserved protein-protein interaction domain of mammalian Lin-2/CASK binds and recruits SAP97 to the lateral surface of epithelia. Mol. Cell Biol. *22*, 1778–1791.

Martin, J.R., and Ollo, R. (1996). A new *Drosophila* $Ca^{2+}$/calmodulin-dependent protein kinase (Caki) is localized in the central nervous system and implicated in walking speed. EMBO J. *15*, 1865–1876.

McCoy, A.J., Grosse-Kunstleve, R.W., Adams, P.D., Winn, M.D., Storoni, L.C., and Read, R.J. (2007). Phaser crystallographic software. J. Appl. Crystallogr. *40*, 658–674.

Moog, U., Kutsche, K., Kortum, F., Chilian, B., Bierhals, T., Apeshiotis, N., Balg, S., Chassaing, N., Coubes, C., Das, S., et al. (2011). Phenotypic spectrum associated with CASK loss-of-function mutations. J. Med. Genet. *48*, 741–751.

Mukherjee, K., Sharma, M., Jahn, R., Wahl, M.C., and Sudhof, T.C. (2010). Evolution of CASK into a $Mg^{2+}$-sensitive kinase. Sci. Signal. *3*, ra33.

Mukherjee, K., Sharma, M., Urlaub, H., Bourenkov, G.P., Jahn, R., Sudhof, T.C., and Wahl, M.C. (2008). CASK functions as a $Mg^{2+}$-independent neurexin kinase. Cell *133*, 328–339.

Murshudov, G.N., Skubak, P., Lebedev, A.A., Pannu, N.S., Steiner, R.A., Nicholls, R.A., Winn, M.D., Long, F., and Vagin, A.A. (2011). REFMAC5 for the refinement of macromolecular crystal structures. Acta Crystallogr. D Biol. Crystallogr. *67*, 355–367.

Najm, J., Horn, D., Wimplinger, I., Golden, J.A., Chizhikov, V.V., Sudi, J., Christian, S.L., Ullmann, R., Kuechler, A., Haas, C.A., et al. (2008). Mutations of CASK cause an X-linked brain malformation phenotype with microcephaly and hypoplasia of the brainstem and cerebellum. Nat. Genet. *40*, 1065–1067.

Olsen, O., Moore, K.A., Fukata, M., Kazuta, T., Trinidad, J.C., Kauer, F.W., Streuli, M., Misawa, H., Burlingame, A.L., Nicoll, R.A., et al. (2005). Neurotransmitter release regulated by a MALS-liprin-alpha presynaptic complex. J. Cell Biol. *170*, 1127–1134.

Otwinowski, Z., and Minor, W. (1997). Processing of X-ray diffraction data collected in oscillation mode. Methods Enzymol. *276*, 307–326.

Rellos, P., Pike, A.C., Niesen, F.H., Salah, E., Lee, W.H., von Delft, F., and Knapp, S. (2010). Structure of the CaMKIIdelta/calmodulin complex reveals the molecular mechanism of CaMKII kinase activation. PLoS Biol. *8*, e1000426.

Rosenberg, O.S., Deindl, S., Sung, R.J., Nairn, A.C., and Kuriyan, J. (2005). Structure of the autoinhibited kinase domain of CaMKII and SAXS analysis of the holoenzyme. Cell *123*, 849–860.

Srivastava, S., McMillan, R., Willis, J., Clark, H., Chavan, V., Liang, C., Zhang, H., Hulver, M., and Mukherjee, K. (2016). X-linked intellectual disability gene CASK regulates postnatal brain growth in a non-cell autonomous manner. Acta Neuropathol. Commun. *4*, 30.

Stafford, R.L., Ear, J., Knight, M.J., and Bowie, J.U. (2011). The molecular basis of the Caskin1 and Mint1 interaction with CASK. J. Mol. Biol. *412*, 3–13.

Stenson, P.D., Ball, E.V., Mort, M., Phillips, A.D., Shiel, J.A., Thomas, N.S.T., Abeysinghe, S., Krawczak, M., and Cooper, D.N. (2003). Human gene mutation database (HGMD®): 2003 update. Hum. Mutat. *21*, 577–581.

Tabuchi, K., Biederer, T., Butz, S., and Südhof, T.C. (2002). CASK participates in alternative tripartite complexes in which Mint 1 competes for binding with Caskin 1, a novel CASK-binding protein. J. Neurosci. *22*, 4264–4273.

Wei, Z., Zheng, S., Spangler, S.A., Yu, C., Hoogenraad, C.C., and Zhang, M. (2011). Liprin-mediated large signaling complex organization revealed by the liprin-alpha/CASK and liprin-alpha/liprin-beta complex structures. Mol. Cell *43*, 586–598.

Won, S., Levy, J.M., Nicoll, R.A., and Roche, K.W. (2017). MAGUKs: multifaceted synaptic organizers. Curr. Opin. Neurobiol. *43*, 94–101.

Zhu, J., Shang, Y., and Zhang, M. (2016). Mechanistic basis of MAGUK-organized complexes in synaptic development and signalling. Nat. Rev. Neurosci. *17*, 209–223.

## STAR★METHODS

### KEY RESOURCES TABLE

| REAGENT or RESOURCE | SOURCE | IDENTIFIER |
|---|---|---|
| Chemicals, Peptides, and Recombinant Proteins | | |
| CASK-CaMK (aa 1-345) | This paper | N/A (custom-made) |
| CASK-CaMK- ΔR1R2 (aa 1-277) | This paper | N/A (custom-made) |
| CASK-CaMK-S64N (aa 1-345, S64N) | This paper | N/A (custom-made) |
| CASK-CaMK-S64I (aa 1-345, S64I) | This paper | N/A (custom-made) |
| CASK-CaMK-R279W (aa 1-345, R279W) | This paper | N/A (custom-made) |
| Mint1-FL (aa 1-842) | This paper | N/A (custom-made) |
| Mint1-N (aa 1-450) | This paper | N/A (custom-made) |
| Mint1-MID-CID (aa 221-450) | This paper | N/A (custom-made) |
| Mint1-CID-a (aa 336-437) | This paper | N/A (custom-made) |
| Mint1-CID-b (aa 378-441) | This paper | N/A (custom-made) |
| Mint1-CID (aa 351-394) | This paper | N/A (custom-made) |
| Mint1-CID-Core (aa 382-394) | This paper | N/A (custom-made) |
| Mint1-CID-Linker-Core (aa 370-394) | This paper | N/A (custom-made) |
| Mint1-CID-αN-Linker (aa 351-381) | This paper | N/A (custom-made) |
| Mint1-CID-W384A (aa 351-394, W384A) | This paper | N/A (custom-made) |
| Mint1-CID-Y374A (aa 351-394, Y374A) | This paper | N/A (custom-made) |
| Mint1-CID-I362E (aa 351-394, I362E) | This paper | N/A (custom-made) |
| CaM (aa 1-149) | This paper | N/A (custom-made) |
| HRV-3C protease | This paper | N/A (custom-made) |
| Deposited Data | | |
| CASK-CaMK/Mint1-CID | This paper | PDB: 6LNM |
| CASK/Liprins-α | (Wei et al., 2011) | PDB: 3TAC |
| CASK/3'-AMP | (Mukherjee et al., 2008) | PDB: 3C0G |
| CaMKII (autoinhibition) | (Rosenberg et al., 2005) | PDB: 2BDW |
| CaMKII (+substrate) | (Chao et al., 2010) | PDB: 3KK8 |
| CaMKII (+CaM+autophosphorylation) | (Rellos et al., 2010) | PDB: 2WEL |
| Experimental Models: Organisms/Strains | | |
| *Escherichia coli* BL21 (DE3) cells | Invitrogen | Cat# C600003 |
| Recombinant DNA | | |
| pET-32a | Novagen | Cat# 69015-3 |
| m3c-CASK-CaMK | This paper | N/A (custom-made) |
| m3c-CASK-CaMK-ΔR1R2 | This paper | N/A (custom-made) |
| m3c-CASK-CaMK-S64N | This paper | N/A (custom-made) |
| m3c-CASK-CaMK-S64I | This paper | N/A (custom-made) |
| m3c-CASK-CaMK-R279W | This paper | N/A (custom-made) |
| 32m3c-Mint1-FL | This paper | N/A (custom-made) |
| 32m3c-Mint1-N | This paper | N/A (custom-made) |
| 32m3c-Mint1-MID-CID | This paper | N/A (custom-made) |
| 32m3c-Mint1-CID-a | This paper | N/A (custom-made) |
| 32m3c-Mint1-CID-b | This paper | N/A (custom-made) |
| 32m3c-Mint1-CID | This paper | N/A (custom-made) |
| 32m3c-Mint1-CID-Core | This paper | N/A (custom-made) |
| 32m3c-Mint1-CID-Linker-Core | This paper | N/A (custom-made) |

(*Continued on next page*)

*Continued*

| REAGENT or RESOURCE | SOURCE | IDENTIFIER |
|---|---|---|
| 32m3c-Mint1-CID-αN-Linker | This paper | N/A (custom-made) |
| 32m3c-Mint1-CID-W384A | This paper | N/A (custom-made) |
| 32m3c-Mint1-CID-Y374A | This paper | N/A (custom-made) |
| 32m3c-Mint1-CID-I362E | This paper | N/A (custom-made) |
| 32m3c-CaM | This paper | N/A (custom-made) |
| Software and Algorithms | | |
| Origin 7.0 | OriginLab | https://www.originlab.com/ |
| ASTRA 6 | Wyatt | http://www.wyatt.com/products/software/astra.html |
| Phaser | (McCoy et al., 2007) | https://smb.slac.stanford.edu/facilities//software/ccp4/html/phaserwiki/index.html |
| Coot | (Emsley et al., 2010) | https://www2.mrc-lmb.cam.ac.uk/personal/pemsley/coot/ |
| Refmac5 | (Murshudov et al., 2011) | https://www2.mrc-lmb.cam.ac.uk/groups/murshudov/content/refmac/refmac.html |
| MolProbity | (Chen et al., 2010) | http://molprobity.biochem.duke.edu/ |
| PyMOL | Schrodinger | http://www.pymol.org/ |
| lollipop | (Jay and Brouwer, 2016) | https://github.com/pbnjay/lollipops |
| Other | | |
| Superdex 75 26/60 | GE Healthcare | Cat# 28-9893-34 |
| ClinVar database | (Landrum et al., 2013) | https://www.ncbi.nlm.nih.gov/clinvar/ |
| Human Gene Mutation Database | (Stenson et al., 2003) | http://www.hgmd.cf.ac.uk/ |
| Cancer Genome Atlas (TCGA) data | (Ellrott et al., 2018) | http://cancergenome.nih.gov/ |

## RESOURCE AVAILABILITY

### Lead Contact

Further information and requests for resources and reagents should be directed to and will be fulfilled by the Lead Contact, Mingjie Zhang (mzhang@ust.hk).

### Materials Availability

This study did not generate new unique reagents.

### Data and Code Availability

The atomic coordinates of the CASK-CaMK and Mint1-CID complex has been deposited to the Protein Data Bank (PDB) with the accession number 6LNM.

## EXPERIMENTAL MODEL AND SUBJECT DETAILS

### Bacterial Strain

*Escherichia coli* BL21-CodonPlus(DE3)-RIL cells (Agilent) were used in this study for the production of recombinant proteins. Cells were cultured in LB medium supplemented with necessary antibiotics.

## METHODS DETAILS

### Constructs, Protein Expression and Purification

The cDNA encoding variant fragments of rat CASK (GenBank: U47110.1) were cloned into a modified pET-32a vector with an N-terminal $His_6$ tag and an HRV-3C protease digestion site. The cDNA encoding human CaM (GenBank: AC006536.2) and variant fragments of mouse Mint1 (GenBank: NM_177034.3) were cloned into a modified pET-32a vector with an N-terminal Trx-$His_6$ tag and an HRV-3C protease digestion site. All constructs were confirmed by DNA sequencing.

All proteins were expressed in *Escherichia coli* BL21-CodonPlus(DE3)-RIL cells (Agilent). The cultures initially grew in LB medium at 37°C until $OD_{600}$ reached 0.6 before addition of 0.25 mM IPTG for induction of protein expression. Typically, protein expression was lasted for 16 h at 16°C. Recombinant proteins were extracted by high pressure homogenizer and purified by using a $Ni^{2+}$-NTA (GE

Healthcare) affinity column followed by size exclusion chromatography using Superdex 75 26/60 (GE Healthcare). The affinity tag of CASK or CaM was cleaved by HRV-3C protease at 4°C overnight and then removed by another step of Superdex 75 26/60 size exclusion chromatography with a buffer containing 50 mM Tris (pH 8.2), 100 mM NaCl, 1 mM DTT, 1 mM EDTA or 50 mM Tris (pH 8.2), 100 mM NaCl, 1 mM DTT, 1 mM $Ca^{2+}$. For Mint1-CID, the Trx-$His_6$ tag was cleaved by HRV-3C protease at 4°C overnight and then removed by another step of mono-Q column. For protein crystallization, CASK-CaMK and Mint1-CID were mixed after HRV-3C digestion, then loaded to a Superdex 75 26/60 column for obtaining the CASK-CaMK/Mint1-CID complex.

### Protein Crystallization and Structure Determination

Crystals of the CASK-CaMK/Mint1-CID complex were obtained by sitting drop vapour-diffusion method at 16°C. CASK-CaMK/Mint1-CID protein complex solution with the concentration of 20 mg/mL was mixed with equal volume (1 μL + 1 μL) of the reservoir buffer containing 0.1 M BisTris (pH 6.0), 20 % (w/v) PEG 1500 for crystallization.

Crystals were cryoprotected with 20 % (v/v) glycerol and flash-cooled to 100 K. X-ray diffraction data were collected at the BL19U1 beamline at the Shanghai Synchrotron Radiation Facility (SSRF). Diffraction data were processed using HKL2000 (Otwinowski and Minor, 1997). The structure was solved by molecular replacement method by Phaser (McCoy et al., 2007) using the structure of CASK-CaMK (PDB ID: 3TAC) as the searching model. Three CASK-CaMK molecules could be found in an asymmetric unit and the electron density of Mint1-CID could be clearly traced. The model of Mint1-CID was manually built using Coot (Emsley et al., 2010). Further model building and refinement were carried out iteratively using Coot and Refmac5 (Murshudov et al., 2011). Since the L-test result indicated merohedral twining of the crystal, twin refinement was used during all rounds of refinement. The final refined twin fractions are 56.98 % for operator H, K, L and 43.02 % for operator -K, -H, -L. The final models were validated by MolProbity (Chen et al., 2010) and statistics were summarized in Table 1. All figures in the paper were prepared using PyMOL (http://www.pymol.org/).

## ISOTHERMAL TITRATION CALORIMETRY (ITC) ASSAY

ITC experiments were performed using a MicroCal VP-ITC calorimeter (Malvern) at 25°C. All proteins used for the ITC assays were individually exchanged to the buffer containing 50 mM Tris (pH 8.2), 100 mM NaCl, 1 mM DTT, 1 mM EDTA or 50 mM Tris (pH 8.2), 100 mM NaCl, 1 mM DTT, 1 mM $Ca^{2+}$ right before each titration experiment. The samples were degassed before loading to the syringe or cell. Each titration point was performed by injecting a 10 μL aliquot of the protein loaded in the syringe into the cell with a duration of 20 s and with an interval time of 150 s to ensure each titration peak fully returned to the baseline. The titration data were fitted with the one-site binding model using Origin 7.0 to derive the $K_d$ values.

### Size Exclusion Chromatography Coupled with Multi-Angle Light Scattering (SEC-MALS) Assay

The SEC-MALS system consists of an AKTA purifier (GE Healthcare), a static light scattering detector (miniDawn Wyatt), and a differential refractive index detector (Optilab, Wyatt). Typically, 100 μl sample (40 μM) was loaded by injection into a Superose 12 10/300 GL column pre-equilibrated with a buffer containing 50 mM Tris (pH 8.2), 100 mM NaCl, 1 mM DTT, 1 mM EDTA or 50 mM Tris (pH 8.2), 100 mM NaCl, 1 mM DTT, 1 mM $Ca^{2+}$. Data were analysed by ASTRA6 (Wyatt).

### Collection of Human Variants Associated with Neurodevelopmental Disorders and Cancer

Variants in the coding sequence of human CASK gene were collected from the ClinVar database (Landrum et al., 2013) and the Human Gene Mutation Database (Stenson et al., 2003). Cancer-related mutations of human CASK gene were obtained from preprocessed variant calls of the Cancer Genome Atlas (TCGA) data (Ellrott et al., 2018). The visualization of variants in CASK protein sequence was produced using lollipop (Jay and Brouwer, 2016).

## QUANTIFICATION AND STATISTICAL ANALYSIS

Information is described in relevant sections of the methods and figure legends.